frontiers | Frontiers in Materials

TYPE Original Research
PUBLISHED 02 April 2024
DOI 10.3389/fmats.2024.1390242

OPEN ACCESS

EDITED BY
Xiangping Hao,
University of Science and Technology Beijing, China

REVIEWED BY
Yuling Zhang,
North China Electric Power University, China
Yang Yu,
Jinan University, China

*CORRESPONDENCE
Chao Song,
songchao@sdu.edu.cn
Shuguang Wang,
wsg@sdu.edu.cn

RECEIVED 23 February 2024
ACCEPTED 19 March 2024
PUBLISHED 02 April 2024

CITATION
Pang B, Li H, Ding C, Song C and Wang S (2024), Synergy effect of polyaspartic acid and D-phenylalanine on corrosion inhibition caused by *Desulfovibrio vulgaris*. *Front. Mater.* 11:1390242. doi: 10.3389/fmats.2024.1390242

Synergy effect of polyaspartic acid and D-phenylalanine on corrosion inhibition caused by *Desulfovibrio vulgaris*

Bo Pang[1,2], Hongyi Li[1,2], Chengcheng Ding[3], Chao Song[1,2]* and Shuguang Wang[1,2,4,5]*

[1]Shandong Key Laboratory of Water Pollution Control and Resource Reuse, School of Environmental Science and Engineering, Shandong University, Qingdao, China, [2]Shandong Key Laboratory of Environmental Processes and Health, School of Environmental Science and Engineering, Shandong University, Qingdao, China, [3]Analytical Testing Center, School of Environmental Science and Engineering, Shandong University, Qingdao, China, [4]Sino-French Research Institute for Ecology and Environment (ISFREE), School of Environmental Science and Engineering, Shandong University, Qingdao, China, [5]WeiHai Research Institute of Industrial Technology of Shandong University, Weihai, China

Microbiologically influenced corrosion (MIC) poses a threat to various fields, particularly in piping and cooling water systems. As a green corrosion inhibitor, polyaspartic acid (PASP) faces challenges in achieving the intended corrosion inhibition against MIC due to biofilm. Therefore, mitigating biofilm might be the key to improving the corrosion inhibition of PASP. D-Phenylalanine (D-Phe) was selected as an enhancer to promote the inhibition of PASP on MIC caused by *Desulfovibrio vulgaris* due to its potential role in biofilm formation in this work. The joint application of PASP and D-Phe reduced the corrosion rate by 76.54% and obviously decreased the depth of corrosion pits with the maximum depth at 0.95 μm. Also, fewer cells adhered to the coupon surface due to the combined action of PASP and D-Phe, leading to thin and loose biofilm. Besides, both cathodic and anodic reactions were retarded with PASP and D-Phe, resulting in a low corrosion current at 0.530×10^{-7} A/cm^2. The primary synergy mechanism is that D-Phe promoted the formation of PASP protective film via decreasing bacterial adhesion and thus inhibited electrochemical reaction and electron utilization of cells from metal surface. This study introduces a novel strategy to augment the effectiveness of PASP in inhibiting MIC.

KEYWORDS

corrosion inhibition, polyaspartic acid, D-amino acids, sulfate-reducing bacteria, biofilm

1 Introduction

Currently, microbiologically influenced corrosion (MIC) poses a threat to various fields, particularly in piping and cooling water systems, constituting a multi-trillion-dollar problem annually (Zhong et al., 2020; Ye et al., 2023; Wang D. et al., 2024). MIC primarily correlated with the biofilm on metal surface (Knisz et al., 2023). Microorganisms within the biofilm generate organic acids, sulfides, and extracellular hydrogenases, facilitating the oxidation of metallic iron (Fe^0) alongside hydrogen (H_2) generation. Some anaerobic microorganisms could utilize H_2 as an electron donor to support anaerobic respiration, while others can directly accept electrons from Fe^0, often

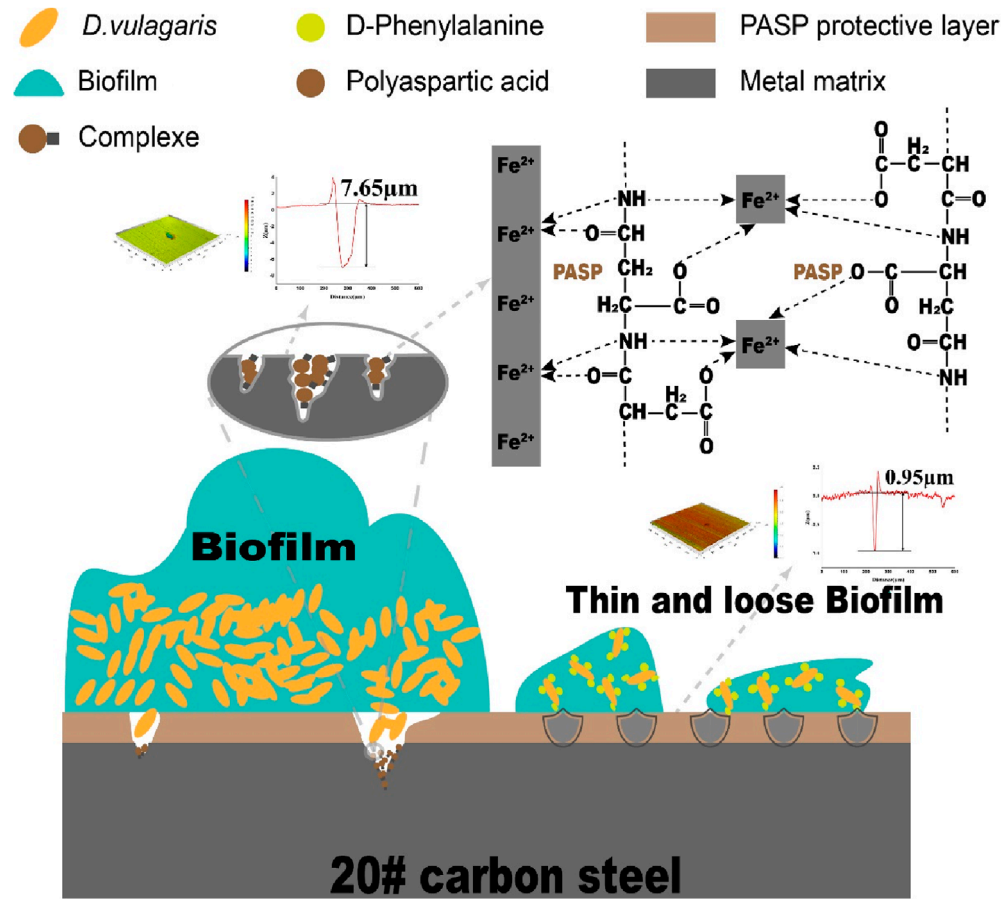

GRAPHICAL ABSTRACT

through c-type cytochromes (Xu et al., 2023). Furthermore, Sulfate-reducing bacteria (SRB) is commonly considered as one of the primary species responsible for MIC in anaerobic environments (Cheng et al., 2024). Metallic iron can serve as the exclusive electron donor for SRB through extracellular electron transfer (EET) during their respiration process (Gu et al., 2019; Pu et al., 2023). Especially, SRB can gain electrons from the pipe surface through the oxidation of metallic iron with sulfate as ultimate electron acceptor (Unsal et al., 2016; Wang et al., 2023). Currently, corrosion inhibitors and biocides are employed to mitigate corrosion in cooling water systems (Hegazy et al., 2014). For example, phosphorus corrosion inhibitors are widely applied due to their low cost and high efficiency. However, the residual phosphorus in effluent lead to eutrophication and algae blooms in natural waters (Rott et al., 2018; Zhu et al., 2021). Innovative corrosion inhibitors and biocides are being developed to replace conventional phosphorus corrosion inhibitors. Wang et al. achieved high corrosion inhibition (>86%) against SRB-induced corrosion using rosin thiourea iminazole quaternary ammonium salt (Wang Q. et al., 2024). However, there are still high risk of environmental problems due to the low biodegradability and high bioaccumulation of some innovative corrosion inhibitors and biocides (Rott et al., 2017; Saverina et al., 2023). Hence, it is necessary to develop green inhibitors for MIC mitigation.

Polyaspartic acid (PASP) is currently regarded as a green corrosion and scale inhibitor due to its non-toxicity and biodegradability (Hasson et al., 2011). PASP can form a protective film on metal surface, thereby effectively obstructing active sites (Qian et al., 2013). Moreover, PASP can work as an anodic inhibitor to reduce metal corrosion (Gao et al., 2015). However, PASP faces challenges in achieving the intended corrosion inhibition when used individually, and the combination with traditional inhibitors greatly decreases the environmental significance of PASP. It is commonly recognized that biofilm plays a pivotal role in MIC, which could disrupt the formation of the protective film by PASP (Vahdati et al., 2022). Besides, various oxygen gradients exist in mature biofilm, which facilitates the proliferation of SRB and thus accelerates electron transfer within metal and corrosion (Jia et al., 2017; Xu et al., 2018). Biocides are frequently utilized to kill microorganisms and enhance the efficiency of corrosion inhibitors. However, biofilm protects cells inside against adverse environment, including biocides, which greatly reduce the efficacy of biocides (Xu et al., 2019). Besides, even with a residual bacterial population as low as 0.01%, biofilm regeneration persists, resulting in escalated expenses and the potential for secondary environmental contamination (Yu et al., 2016). Therefore, biofilm reduction is crucial for improving the corrosion inhibition of PASP.

D-amino acids are naturally occurring organic compounds found in plants, microorganisms, and even within human body (Aliashkevich et al., 2018). They could regulate peptidoglycan to change the chemical properties of cell walls (Cava et al., 2011). Besides, they also exhibit inhibition on biofilm formation via interfering with the signaling molecules that control bacterial adhesion (Xu and Liu, 2011; Li et al., 2021; Li et al., 2023). For example, Kolodkin-Gal et al. found the dispersal of *S. aureus* and *B. subtilis* biofilms with the addition of D-amino acids, and Kao et al. reported the inhibition of D-amino acids on *P. aeruginosa* biofilm formation (Kolodkin-Gal et al., 2010; Kao et al., 2017). Besides, the membrane incorporating immobilized D-amino acids exhibited significant inhibition on initial bacterial adhesion and biofilm formation (Jiang et al., 2017; Yu et al., 2018). Hence, D-amino acids might serve as potential enhancers for PASP on MIC. It is crucial to explore the synergy effect of PASP and D-amino acid on MIC from both economic and environmental perspectives.

In this study, a strain of sulfate-reducing bacteria (SRB), *Desulfovibrio vulgaris*, was employed, and D-phenylalanine (D-Phe) was chosen as a representative D-amino acid to systematically evaluate its roles in improving the corrosion inhibition of PASP. The corrosion of 20# carbon steel caused by *D. vulgaris* was assessed through weight loss analysis, scanning electron microscopy (SEM), and confocal laser scanning microscope (CLSM). The objectives of this study were to assess the impact of D-Phe and PASP on MIC, as well as to explore the synergy mechanism on corrosion inhibition. To our current understanding, this is the first investigation to explore the synergy mechanism of PASP and D-Phe in SRB-mediated corrosion. This work provides new insights into enhancing green inhibitors and reducing their negative environmental impact.

2 Materials and methods

2.1 Bacterium, culture medium, and chemicals

Desulfovibrio vulgaris ATCC 7757, a strain of SRB utilized in this study, was obtained from the General Microbiological Culture Collection Center in China. The ATCC 1249 medium (Supplementary Text S1) was used for bacterial cultivation (Jia et al., 2018a). The medium underwent a 40-min deoxygenation process using N_2 and was subsequently autoclaved at 121°C for 25 min. Additionally, L-cysteine (100 mg/L, Macklin, Shanghai, AR>98%) was introduced as an oxygen scavenger (Jia et al., 2018b). D-Phe (Macklin, Shanghai, AR>98%) and PASP (Macklin, Shanghai, AR > 95%) were dissolved in deionized water and used after filtration with 0.22 μm filters. The information on growth curve was provided in Supplementary Text S2.

2.2 Operation of the reactor and weight loss measurement

The microbial corrosion was evaluated in four reactors. The dimensions of each reactor were 92 mm in height, 60 mm in inner diameter, and a volume of 200 mL (Supplementary Figure S1). Eight 20# carbon steel coupons (10 × 10 × 3 mm), a commonly used material in industrial pipelines, were placed in each reactor. The elemental composition of the carbon steel is presented in Supplementary Table S1. The coupons first underwent a sequential grinding process using silicon carbide paper with varying grit sizes (220, 400, 800, 2000) and then received ultraviolet light exposure for 30 min to ensure sterilization (Jia et al., 2018b). Subsequently, all coupons were firmly secured in rubber sleeves within the reactors. The SRB was cultured in reactors with a medium that included PASP, D-Phe, and PASP + D-Phe, denoted as PASP, D-Phe, and P + D group, respectively. The concentrations of PASP and D-Phe were 40 mg/L and 10 mg/L according to our previous study, respectively (Gong et al., 2023). A blank group was prepared without the addition of PASP and D-Phe. Additionally, an abiotic group was designed without SRB. All reactors were incubated at 30°C for 14 days.

After 14-day incubation, the coupons underwent a treatment to remove biofilm and corrosion products according to the ASTM G1-03 standard (Zhang B. et al., 2015). Subsequently, the coupons underwent three rounds of cleaning with anhydrous alcohol, followed by drying in a vacuum oven at 60°C. Then, the weight loss was calculated via measuring the difference in mass of the coupons before and after the incubation. In each reactor, four coupons were prepared for weight measurement, the average weight loss was calculated for each data point, and the average corrosion rate (V) and inhibition rate (η) were determined using the following formulas:

$$V = \frac{8760 \times 10 \times (m - m_0)}{A \bullet T \bullet \rho} \tag{1}$$

$$\eta = \frac{v_0 - v_1}{v_0} \times 100\% \tag{2}$$

where V is the corrosion rate (mm/a). m is the mass reduction of the coupons. m_0 is the average weight loss of the blank test for the acid etching of the test coupons (g). A is the coupon surface area (cm^2). T is the incubation time (h). ρ is the density of the coupon (g/cm^3). v_0 is the corrosion rate in blank group and v_1 is the corrosion rate in other groups.

Additionally, a synergy parameter (S) was determined in terms of corrosion activities according to Aramaki–Hackerman model:

$$S = \frac{1 - \eta_{Atamaki}^{threshold}}{1 - \eta^{measured}} \tag{3}$$

where $\eta^{threshold}$ is the threshold inhibition efficiency. $\eta^{measured}$ is the evaluated mixture's inhibition efficiency. $S > 1$ indicates synergism, and $S < 1$ indicates antagonism (Aramaki and Hackerman, 1969; Kozlica et al., 2021; Kokalj, 2023).

2.3 Corrosion morphology and corrosion products

After the incubation, the coupons with biofilm were collected and rinsed with phosphate-buffered saline (PBS, pH = 7.4) three times to clear the residual medium. Then, the coupons were fixed

with 2.5% glutaraldehyde in PBS solution for 2 h and washed with PBS solution three times, followed by dehydration. Ultimately, the coupons were dried in a CO_2 dryer, and subsequent to this, palladium coating was applied to enhance conductivity before conducting SEM (Quanta 250 FEG, FEI, United States of America) analysis. The coupons were subjected to pretreatment to remove biofilm prior to SEM analysis to observe the pitting corrosion morphology. Subsequently, corrosion pits of coupons were observed and analyzed with a confocal laser scanning microscope (CLSM, LSM 800, Carl Zeiss, Germany) and ZEISS ConfoMap software, respectively (Li et al., 2021). Each sample was scanned in 10 regions to find the maximum pit depth. In addition, the corrosion products were collected, and the composition of sulfur-related components was recorded with X-ray photoelectron spectroscopy (XPS, Thermo Fisher Nexsa, United States of America). The XPS spectra was analyzed with Avantage software and the XPS reference binding energies (B.E.) of sulfur species were listed in Supplementary Table S2.

CLSM was also applied to observe cells in biofilm. Briefly, the collected coupon containing biofilm was gently washed using PBS solution and stained using SYTO 9 (live cells) and PI (dead cells) stain. Stained coupons were incubated in dark for 20 min to ensure optimal staining, after which the coupons were carefully washed using a PBS solution again to remove excess stain and to enhance the clarity of observations. Finally, the coupons were observed with CLSM (LSM 900, Carl Zeiss, Germany), and the images were obtained with ZEISS ZEN 3.7 software. ImageJ software was employed to measure the total fluorescence intensity of each image, and the relative amounts of cells were calculated in comparison with in blank group.

2.4 Electrochemical tests

The incubation, while maintaining stringent control over experimental conditions, was reproduced in three-electrode cells. The platinum sheet functioned as the counter electrode. Carbon steel, with a 1 cm^2 exposed surface, served as the working electrode, and Ag/AgCl (KCl-saturated) was used as the reference electrode. The open circuit potential (OCP) and Electrochemical Impedance Spectroscopy (EIS) were measured at 1, 3, 6, 10, and 14 days, and potentiodynamic polarization tests were conducted at 14 days using an electrochemical workstation (CHI 660e, CH Instruments Inc., United States of America). The EIS measurement was conducted at the OCP using a sinusoidal signal with an amplitude of 10 mV, covering a frequency range from 100,000 Hz–0.01 Hz. The EIS data were fitted with ZsimpWin software. Additionally, the Tafel curve was automatically recorded at a scanning rate of 0.167 mV/s, ranging from −0.25 V to +0.25 V vs. the OCP.

2.5 Statistical analysis

The difference among samples were assessed employing the SPSS software through one-way ANOVA, and the levels of significance were denoted by *p*-values less than 0.05.

3 Results and discussion

3.1 Corrosion analysis

Weight loss was first measured and corrosion rates were calculated to assess corrosion. As shown in Figure 1, the corrosion rate increased from 0.018 mm/a in abiotic group to 0.034 mm/a in blank group, confirming that SRB can cause serious metal corrosion. Less weight loss was observed in both PASP group and D-Phe group with corrosion rates at 0.017 mm/a and 0.024 mm/a, respectively. The corrosion inhibition by D-Phe might be attributed to that D-Phe decreased the initial attachment of SRB on coupons, consequently limiting the consumption of iron by SRB. Besides, the corrosion greatly reduced in P + D group, with the corrosion rate decreasing by 76.54% than that in blank group. In previous studies, a corrosion inhibition of 80% was attained with the application of 4000 mg/L PASP, which is 100 times than our used dosage (Cui et al., 2011). Besides, Zeino et al. achieved high corrosion inhibition at 97% through the joint application of 500 mg/L PASP and 10 mg/L zinc ions (Zeino et al., 2018). In this study, a remarkable corrosion inhibition, up to 76.54%, was achieved with low doses of PASP (40 mg/L) and D-Phe (10 mg/L), both of which are non-toxic and biodegradable. Furthermore, according to the Aramaki-Hackerman model, the synergy parameter S was 1.48, indicating the synergism between D-Phe and PASP on corrosion inhibition.

After incubation, the coupons were cleaned to remove attached cells and observed with SEM and CLSM. Serious corrosion was detected on coupons surface in blank group with a huge area and depth at 7.65 μm (Figure 2A, A′). In the D-Phe group, some small and shallow-depth pits were observed, and the maximum depth was 3.26 μm (Figure 2C, C′), suggesting that D-Phe could alleviate pitting corrosion. Moreover, few deep pits were detected in PASP group and P + D group (Figures 2B,D) with maximum depths at 1.44 and 0.95 μm, respectively (Figures 2B', D'). Typically, ferrite on the iron coupons is more susceptible to corrosion than cementite (Li et al., 2021; Li et al., 2023). It can be explained that cementite contains covalent bonds, which reduce electron activity and make it difficult for bacteria to utilize electrons (Hao et al., 2016; Liu et al., 2021). In this study, the joint application of PASP and D-Phe led to a decrease in the depth of pitting corrosion, consequently preventing the exposure of ferrite, ultimately resulting in fewer electrons lost from the coupons and utilized by SRB. These results are consistent with corrosion rates and confirm the synergetic role of PASP and D-Phe in corrosion inhibition.

Hydrogen sulfide and other sulfides, the corrosive products formed during the reduction of sulfate by SRB, play an important role in metal corrosion by *Desulfovibrio vulgaris* in anaerobic environments (Yuan et al., 2013). In this study, XPS analysis was performed on the sulfur components in corrosion products (Supplementary Figure S2). After a 14-day incubation, the curve-fitted S 2p spectra indicated a complex mixture of sulfur species. The peak of SO_4^{2-} is likely attributed to the sulfate deposition from the culture medium (Pu et al., 2023). In P + D group, the relative amount of SO_4^{2-}, serving as the ultimate electron acceptor for SRB, is the highest. It may be attributed to the lower biofilm formation observed on coupon in the P + D group, as discussed

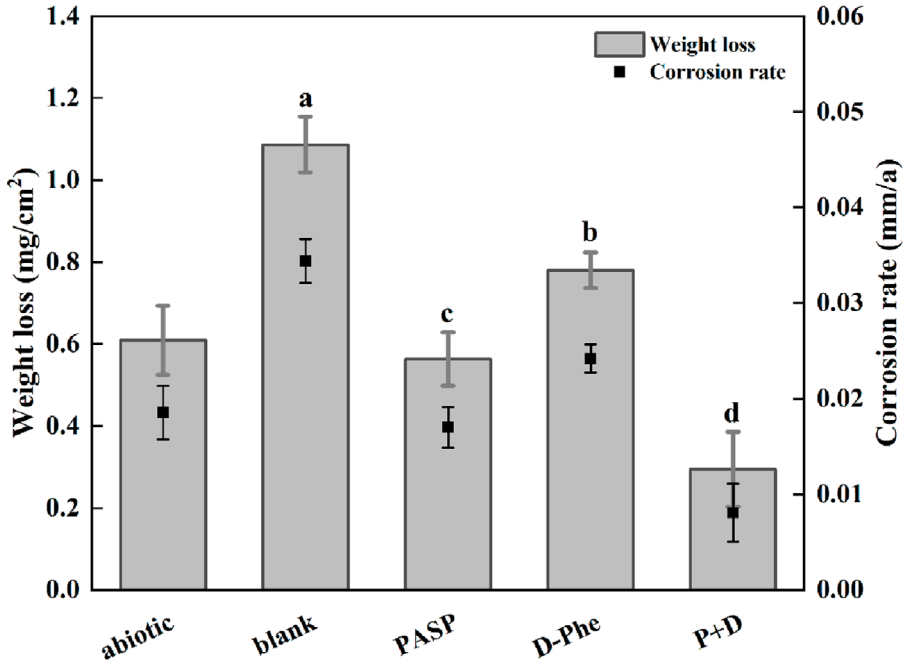

FIGURE 1
Weight loss and corrosion rate in different corrosion conditions for 14 days. The dates were analyzed using one-way ANOVA, and the different letters indicate significant differences between different groups ($p < 0.05$).

in subsequent sections. Furthermore, the presence of organic sulfides implies that biologically derived organic proteins are likely contributing to the generation of sulfide species within the passive films (Yuan et al., 2013).

3.2 SRB growth and biofilm analysis

SRB could attach to the coupons, utilize the electrons, and cause MIC (Jia et al., 2019). Therefore, biomass on the coupons is an important factor for MIC, which directly determines the utilization of electrons by SRB (Vahdati et al., 2022). Therefore, this study evaluated the growth of SRB in the presence of PASP and D-Phe. The growth curves exhibited a remarkably close overlap in all groups (Supplementary Figure S3), suggesting that both PASP and D-Phe showed negligible impact on the growth of SRB. Based on this, it was speculated that the joint application of PASP and D-Phe primarily reduced corrosion via inhibiting the attachment of SRB rather than inhibiting SRB growth. Therefore, SEM and CLSM were employed to observe the biofilm on the coupons. As shown in Figure 3A and Supplementary Figure S4A, the coupons in blank group exhibited complete coverage by biofilm and corrosion products after 14-day incubation. Biofilms with varying sizes and shapes were observed with large patchy and mushroom-like structures. The cells within the biofilm were tightly embedded, displaying a high degree of alignment and minimal open gaps. Moreover, the biofilm was looser, thinner, and contained significantly more gaps in D-Phe group (Figure 3C). Also, the cellular morphology with the addition of D-Phe was different from that in blank group, aligning with other studies (Li et al., 2018; Li et al., 2021). D-Phe can alter cell morphology via substituting the original D-amino acids in peptidoglycan, which serves as a cell wall framework (Dramsi et al., 2008; Lam et al., 2009; Kolodkin-Gal et al., 2010; Carniello et al., 2018). It also affects the synthesis of flagella and adhesion-like proteins, which contribute to initial bacterial attachment and irreversible adherence, respectively (Clark et al., 2007; Karatan and Watnick, 2009; Zhang et al., 2021). Furthermore, the presence of non-uniform bacterial shapes would diminish the efficacy of biofilm formation (Young, 2006). It might be a reason that D-Phe reduced the corrosion by SRB.

Moreover, cells were sparser on the coupon in PASP group (Figure 3B), and fewer corrosion products were observed than those in blank group, which might be attributed to the protective film formed by PASP (Supplementary Figure S4B). Generally, PASP can attach to the surface of coupon in a parallel orientation via carboxyl groups and amide groups in polymer chain to form a dense protective film (Zeino et al., 2018). The functional groups in PASP can complex with iron ions and prevent their further participation in corrosion reactions, and thus inhibit the dissolution of metal ions (anodic reaction) (Xu et al., 2016; Jia et al., 2019). Besides, the protective film effectively obstructs the reaction sites for H^+ ions, leading to the inhibition of the hydrogen evolution reaction (cathodic reaction) (Qian et al., 2013). In this study, PASP might also impede direct contact between SRB and the carbon steel surface, decreasing the electron utilization of SRB from coupon. It is because *D. vulgaris* primarily accepts electrons from Fe^0 through H_2, which serves as an intermediary electron carrier (Wang et al., 2020; Woodard et al., 2023). Furthermore, in P + D group, almost no biofilm and little corrosion products were found (Figure 3D), resulting from the combined effect of PASP and D-Phe. It is consistent with results in weight loss measurements.

10.3389/fmats.2024.1390242

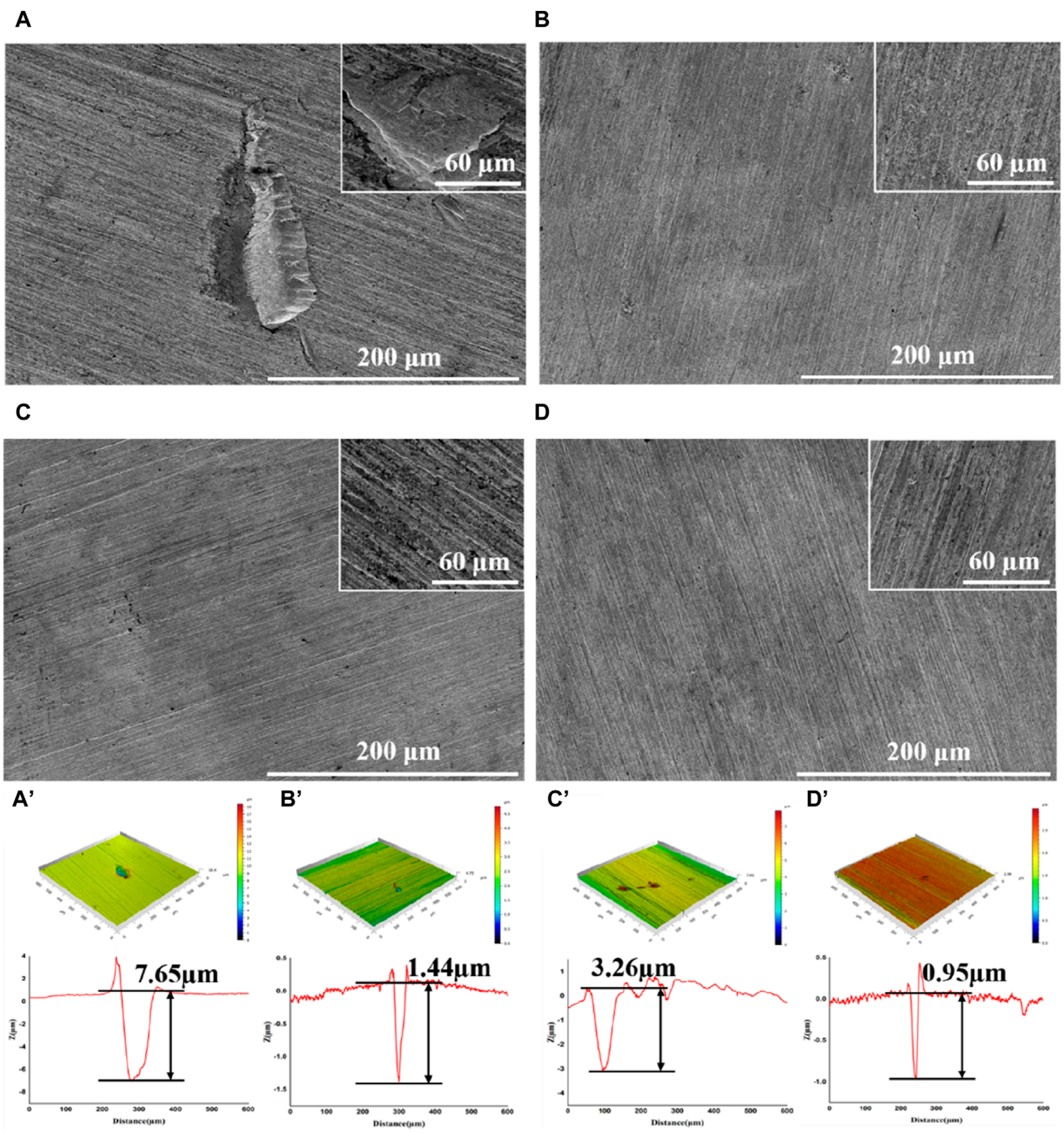

FIGURE 2
SEM images and CLSM pit depth profile of coupons after removal of the biofilm following a 14-day immersion in different corrosion conditions: blank group **(A,A′)**, PASP group **(B,B′)**, D-Phe group **(C,C′)** and P + D group **(D,D′)**.

CLSM was employed to evaluate the distribution of cells on the coupon (Figure 3A'–D'). Live cells (green) were obviously observed while there were almost no dead cells (red) on the coupon in all groups, confirming the minimal effect of PASP and D-Phe on SRB growth. Furthermore, fluorescence intensities were recorded to evaluate the relative amounts of adhered cells. Compared to blank group, the amounts of adhered cells in PASP group reduced by 64%, which might be due to the protective film formed by PASP. Besides, it reduced by 82% and 96% in D-Phe and P + D groups, respectively, confirming that D-Phe could inhibit bacterial adhesion.

3.3 Electrochemical analysis

The OCP tests were first performed (Figure 4A). On Day 1, the OCP values were at a low level in all groups, resulting from minimal bacterial adhesion on the coupon surface (Starosvetsky et al., 2000).

10.3389/fmats.2024.1390242

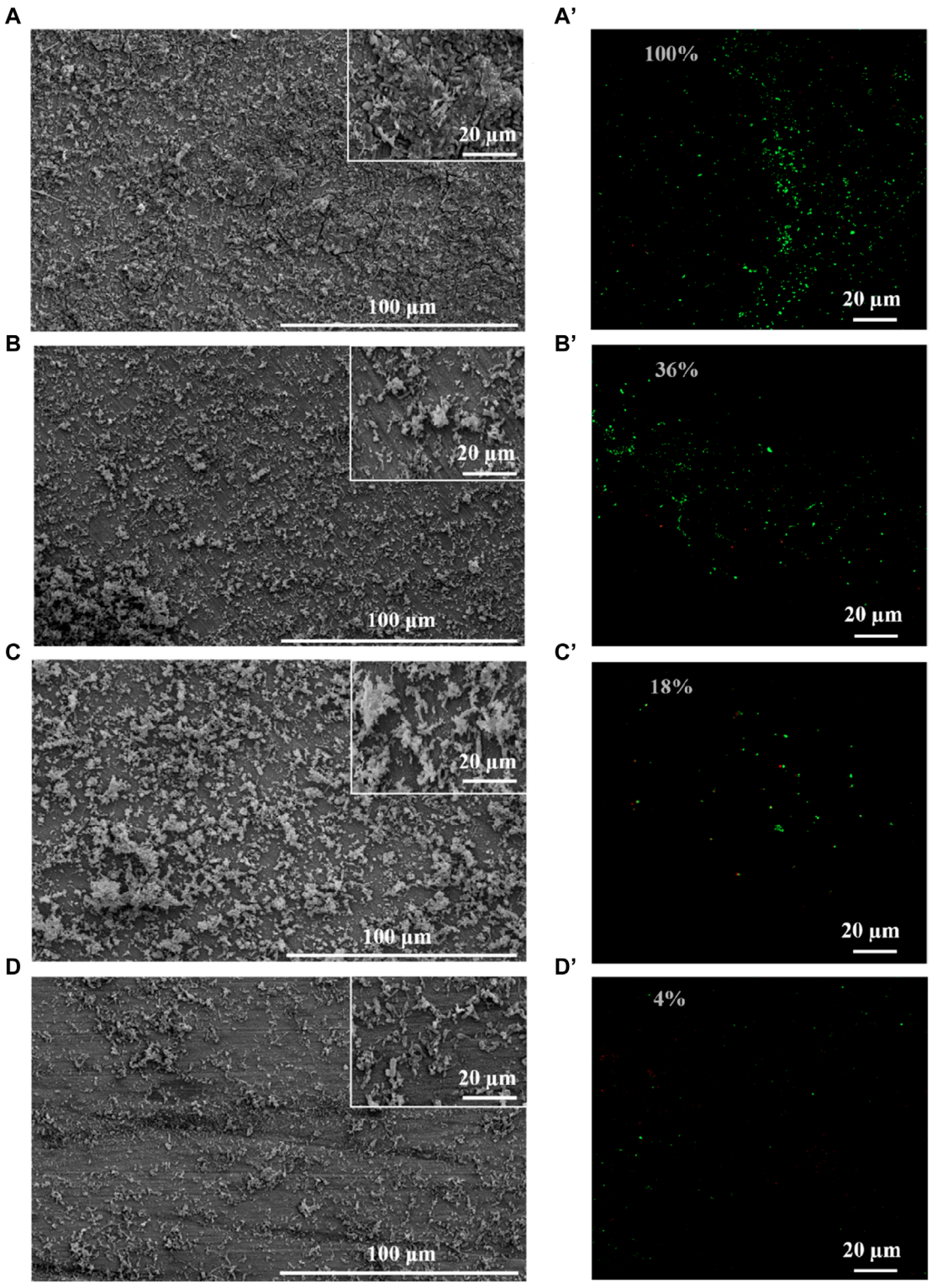

FIGURE 3
SEM and CLSM images of biofilm after 14-day immersion in different corrosion conditions: blank group **(A,A′)**, PASP group **(B,B′)**, D-Phe group **(C,C′)** and P + D group **(D,D′).** The semi-transparent numbers represent the relative amounts of adhered cells.

Higher OCP values were detected in the presence of PASP, indicating high resistance to corrosion, which might be due to the protective film formed by PASP. Then, the values increased sharply on Day 3 due to the formation of FeS-biofilm (FeS film underneath the biofilm) on the coupon surface (Xu et al., 2019). Besides, there were higher OCP values in D-Phe group and PASP group at

10.3389/fmats.2024.1390242

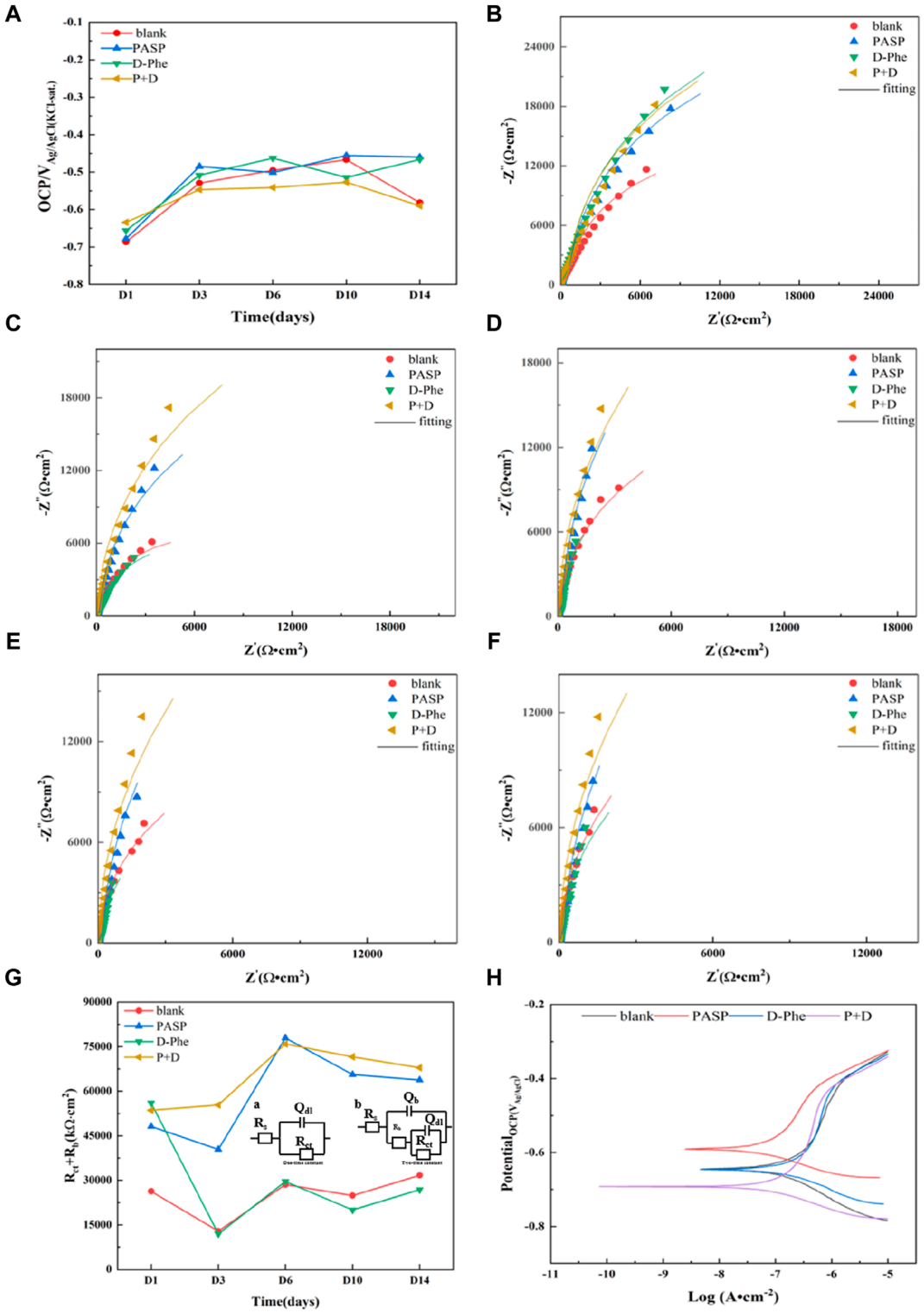

FIGURE 4
Open circuit potential **(A)**, Nyquist plots **(B–F)**, $R_{ct} + R_b$ **(G)**, potentiodynamic polarization curves **(H)** of coupons at different times: **(B)** 1 day, **(C)** 3 days, **(D)** 6 days, **(E)** 10 days, **(F)** 14 days.

most time during incubation than those in blank group, implying a higher resistance to corrosion (Vasudevan et al., 1998; Li et al., 2021). These results indicated that D-Phe and PASP reduced the electron utilization of SRB from coupon, corresponding to weight loss measurement. For the P + D group, the values of OCP did not change dramatically and were always lower than other groups. It can

TABLE 1 Electrochemical parameters of potentiodynamic polarization curves in different groups.

	Ep (V)	I_{corr} (x10^{-7} A·cm^{-2})	b_a (V·dec^{-1})	b_c (V·dec^{-1})
Blank	−0.645	1.863	3.573	11.784
PASP	−0.591	0.630	6.265	20.478
D-Phe	−0.646	1.644	2.940	21.727
P + D	−0.692	0.530	9.422	35.027

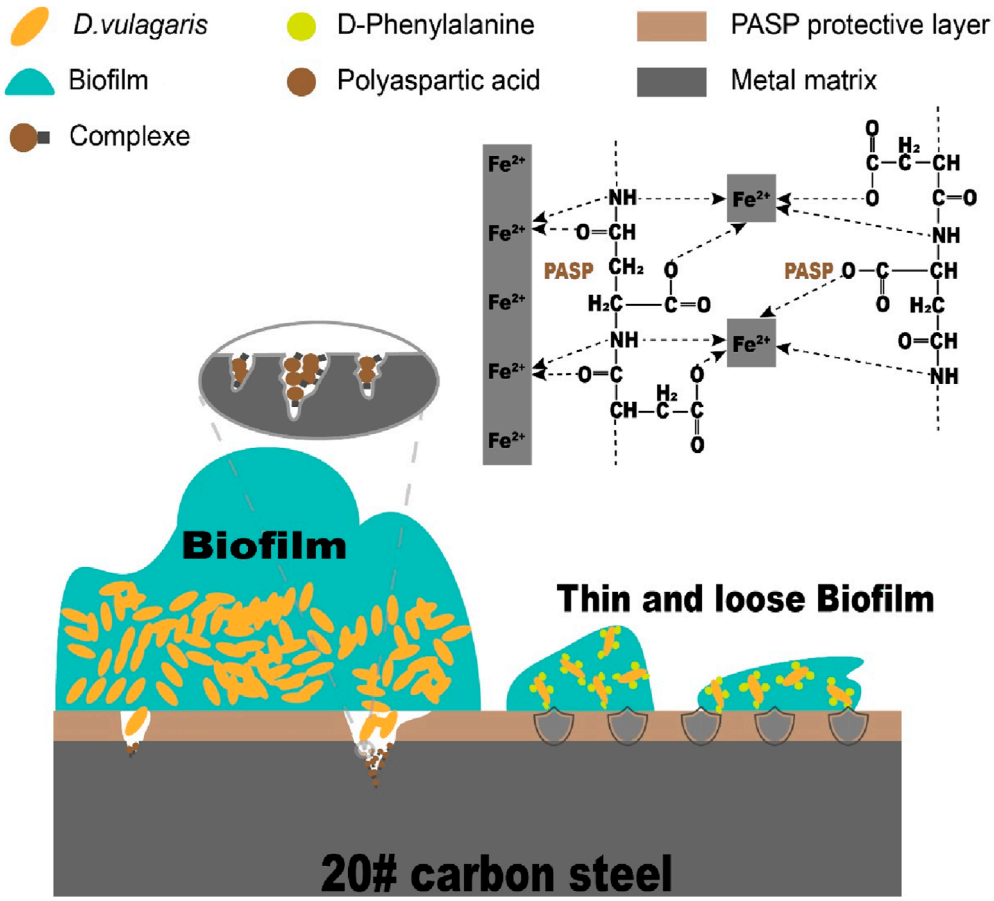

FIGURE 5
Schematic diagram of synergy mechanisms of PASP and D-Phe on corrosion inhibition.

be explained by the combined effect of PASP and D-Phe, resulting in minimal formation of the FeS-biofilm on the coupon surface throughout the entire 14-day incubation (Xu et al., 2019).

EIS was then measured with stable OCP on Day 1, 3, 6, 10, and 14, and the Nyquist plot was used to assess the corrosion (Figures 4B–F), where the diameter in the Nyquist plot is correlated with the corrosion resistance (Gamry Instruments, 2007). On day 1, the diameters were much larger in other groups compared to blank group, which is consistent with OCP values. Moreover, the diameters in P + D group were consistently larger than those in other groups, indicating that the coupon in P + D group exhibited the highest corrosion resistance during the incubation, confirming the synergy effect between PASP and D-Phe on corrosion inhibition. Furthermore, equivalent electrical circuits were employed to fit the impedance spectra (San et al., 2014). The equivalent electrical circuits involved parameters R_s (solution resistance), Q_{dl} (double film capacitance), R_{ct} (charge transfer resistance), Q_b (biofilm capacitance), and R_b (biofilm resistance). The values of R_{ct} + R_b are shown in Figure 4G. There is a close correlation between R_{ct} + R_b value and corrosion rate, where a lower R_{ct} + R_b value corresponds to a higher corrosion rate. Compared to blank group, the R_{ct} + R_b values in other groups were similar but obviously higher on Day 1, indicating that the corrosion rates in PASP group, D-Phe group, and P + D group were close but lower than those

in blank group. After 6 days-incubation, compared to the blank group, the R_{ct} + R_b values in D-Phe group were lower, which might be due to a larger exposed electrode area and a thinner FeS-biofilm on coupon surface. These results could be attributed to two reasons. Firstly, the D-Phe impeded the initial attachment of bacteria, thus reducing the biofilm formation (Carniello et al., 2018). Consequently, the coupon in D-Phe group displayed high corrosion resistance on Day 1, which is consistent with results in Figures 4A, B. Secondly, D-Phe induced cell wall deformation and weakened cell-to-cell connections, ultimately resulting in the collapse of the biofilm (Beech and Sunner, 2004; Castaneda and Benetton, 2008; AlAbbas et al., 2013; Bucher et al., 2015). There were high R_{ct} + R_b values in the presence of PASP, indicating that PASP enhanced the charge transfer resistance of coupons and thus decreased the corrosion rate. It also verified the existence of protective film formed by PASP. Moreover, the R_{ct} + R_b values were highest at most time during incubation in P + D group, confirming the synergy effect of PASP and D-Phe.

Potentiodynamic polarization tests were also conducted on Day 14 to evaluate the corrosion (Figure 4H), and the parameters related to potentiodynamic polarization tests were listed in Table 1. The polarization curves in PASP group and P + D group exhibited distinct variations in comparison with that in blank group, suggesting disparate reaction kinetics of the anode and cathode process. It might be attributed to the change in the electron transfer process, which was caused by attached SRB and PAPS protective film (Valcarce and Vazquez, 2010; Zhang et al., 2011; Farag and Hegazy, 2013; Zhang P. et al., 2015; Lv et al., 2022). Typically, there is a positive correlation between corrosion current and corrosion rate (Chilkoor et al., 2018). Tafel curves of both anodic and cathodic in P + D group shifted to lower corrosion current at 0.530×10^{-7} A cm^{-2}, significantly lower than that in blank group (1.863×10^{-7} A cm^{-2}), indicating that the joint application of PASP and D-Phe decreased corrosion rate. For D-Phe group, the corrosion current at 1.644×10^{-7} A cm^{-2} was close to that in blank group, and the polarization curve on Day 14 was also similar to that in blank group, which might be attributed to the weak effect of D-Phe due to its decomposition over 14 days. These results correspond with weight loss measurement.

3.4 Synergy mechanism of PASP and D-Phe on corrosion inhibition

Based on the preceding discussion and results, the possible synergy mechanism of PASP and D-Phe on corrosion inhibition was summarized in Figure 5. In particular, PASP adsorbed onto the surface of coupons to form a compact protective film. This film acted as a barrier, obstructing the active sites on the coupons and inhibiting direct interaction between SRB and iron on coupon surface (Qian et al., 2013). As a result, the protective film obstructed the electron uptake by SRB from the elemental iron. Nevertheless, as the biofilm forms on the surface of the protective film, the cells within the biofilm instigated a significant challenge to the integrity of this protective film. Upon the rupture of this protective film, the corrosion is initiated, leading to the release of iron ions. The released iron ions at the corrosion sites on the carbon steel surface interacted with PASP to form complexes, effectively hindering the dissolution of metal ions. Additionally, D-Phe effectively suppressed the initial bacterial adhesion, notably extending the period for SRB to establish biofilms on the protective film. During the biofilm formation, D-Phe induced the deformation of cell walls, along with the attenuation of intercellular connections, leading to the collapse of biofilm. Thin and loose biofilms significantly diminished their aggressiveness towards the protective film. Consequently, the presence of D-Phe obviously enhanced both the efficiency and duration of PASP on corrosion inhibition.

4 Conclusion

In this work, the synergy effect of PASP and D-Phe was assessed on MIC induced by *Desulfovibrio vulgaris*. The joint application of D-Phe and PASP significantly reduced corrosion rate and the depth of corrosion pits. Besides, both cathodic and anodic reactions were retarded in the presence of D-Phe and PASP, leading to low corrosion current. The possible synergy mechanism is: (1) PASP formed a protective film to inhibit the corrosion via reducing electrochemical reaction and impeding direct contact between SRB and carbon steel surface; (2) D-Phe decreased the bacterial adhesion, retarded biofilm formation and thus decreased electron utilization of SRB from coupon; (3) D-Phe promoted the formation of protective film by PASP via reducing initial bacterial adhesion. This study provides a novel approach to augment the effectiveness of PASP in MIC inhibition and is helpful to reduce the adverse environmental impact caused by traditional corrosion inhibitors.

Data availability statement

The original contributions presented in the study are included in the article/Supplementary Material, further inquiries can be directed to the corresponding authors.

Author contributions

BP: Formal Analysis, Investigation, Methodology, Writing–original draft, Writing–review and editing. HL: Formal Analysis, Methodology, Writing–original draft, Writing–review and editing. CD: Formal Analysis, Methodology, Writing–review and editing. CS: Conceptualization, Formal Analysis, Methodology, Resources, Supervision, Writing–original draft, Writing–review and editing. SW: Conceptualization, Resources, Supervision, Writing–review and editing.

Funding

The author(s) declare financial support was received for the research, authorship, and/or publication of this article. This work was supported by the National Natural Science Foundation of China (U20A20146 and 22378232), the Young Scholars Program of Shandong University, and Taishan Scholars Project of Shandong Province (No. tstp20230604).

Acknowledgments

We thank Qiang Li from Shiyanjia Lab (www.shiyanjia.com) for XPS analysis. We thank Haiyan Yu, Xiaomin Zhao, and Yuyu Guo, Sen Wang from Core Facilities for Life and Environmental Sciences of SKLMT (State Key Laboratory of Microbial Technology, Shandong University) for CLSM and SEM analysis.

Conflict of interest

The authors declare that the research was conducted in the absence of any commercial or financial relationships that could be construed as a potential conflict of interest.

Publisher's note

All claims expressed in this article are solely those of the authors and do not necessarily represent those of their affiliated organizations, or those of the publisher, the editors and the reviewers. Any product that may be evaluated in this article, or claim that may be made by its manufacturer, is not guaranteed or endorsed by the publisher.

Supplementary material

The Supplementary Material for this article can be found online at: https://www.frontiersin.org/articles/10.3389/fmats.2024.1390242/full#supplementary-material

References

AlAbbas, F. M., Williamson, C., Bhola, S. M., Spear, J. R., Olson, D. L., Mishra, B., et al. (2013). Influence of sulfate reducing bacterial biofilm on corrosion behavior of low-alloy, high-strength steel (api-5l x80). *Int. Biodeterior. Biodegrad.* 78, 34–42. doi:10.1016/j.ibiod.2012.10.014

Aliashkevich, A., Alvarez, L., and Cava, F. (2018). New insights into the mechanisms and biological roles of d-amino acids in complex eco-systems. *Front. Microbiol.* 9, 683. doi:10.3389/fmicb.2018.00683

Aramaki, K., and Hackerman, N. (1969). Inhibition mechanism of medium-sized polymethyleneimine. *J. Electrochem Soc.* 116, 568. doi:10.1149/1.2411965

Beech, W. B., and Sunner, J. (2004). Biocorrosion: towards understanding interactions between biofilms and metals. *Curr. Opin. Biotechnol.* 15, 181–186. doi:10.1016/j.copbio.2004.05.001

Bucher, T., Oppenheimer-Shaanan, Y., Savidor, A., Bloom-Ackermann, Z., and Kolodkin-Gal, I. (2015). Disturbance of the bacterial cell wall specifically interferes with biofilm formation. *Environ. Microbiol. Rep.* 7, 990–1004. doi:10.1111/1758-2229.12346

Carniello, V., Peterson, B. W., van der Mei, H. C., and Busscher, H. J. (2018). Physico-chemistry from initial bacterial adhesion to surface-programmed biofilm growth. *Adv. Colloid Interface Sci.* 261, 1–14. doi:10.1016/j.cis.2018.10.005

Castaneda, H., and Benetton, X. D. (2008). Srb-biofilm influence in active corrosion sites formed at the steel-electrolyte interface when exposed to artificial seawater conditions. *Corros. Sci.* 50, 1169–1183. doi:10.1016/j.corsci.2007.11.032

Cava, F., Lam, H., de Pedro, M. A., and Waldor, M. K. (2011). Emerging knowledge of regulatory roles of d-amino acids in bacteria. *Cell Mol. Life Sci.* 68, 817–831. doi:10.1007/s00018-010-0571-8

Cheng, J., Wu, Y., Duan, J., Polat, G., Hong, S., and Cheng, J. (2024). The influence of srb on corrosion behavior of cu-based medium-entropy alloy coating sprayed by hvof. *Bioelectrochemistry Amst. Neth.* 156, 108633. doi:10.1016/j.bioelechem.2023.108633

Chilkoor, G., Karanam, S. P., Star, S., Shrestha, N., Sani, R. K., Upadhyayula, V. K. K., et al. (2018). Hexagonal boron nitride: the thinnest insulating barrier to microbial corrosion. *Acs Nano* 12, 2242–2252. doi:10.1021/acsnano.7b06211

Clark, M. E., Edelmann, R. E., Duley, M. L., Wall, J. D., and Fields, M. W. (2007). Biofilm formation in desulfovibrio vulgaris hildenborough is dependent upon protein filaments. *Environ. Microbiol.* 9, 2844–2854. doi:10.1111/j.1462-2920.2007.01398.x

Cui, R., Gu, N., and Li, C. (2011). Polyaspartic acid as a green corrosion inhibitor for carbon steel. *Mater. Corros.* 62, 362–369. doi:10.1002/maco.200905511

Dramsi, S., Magnet, S., Davison, S., and Arthur, M. (2008). Covalent attachment of proteins to peptidoglycan. *Fems Microbiol. Rev.* 32, 307–320. doi:10.1111/j.1574-6976.2008.00102.x

Farag, A. A., and Hegazy, M. A. (2013). Synergistic inhibition effect of potassium iodide and novel schiff bases on x65 steel corrosion in 0.5 m h2so4. *Corros. Sci.* 74, 168–177. doi:10.1016/j.corsci.2013.04.039

Gamry Instruments (2007). *Basics of electrochemical impedance spectroscopy, complex impedance in corrosion*, 1–30.

Gao, Y., Fan, L., Ward, L., and Liu, Z. (2015). Synthesis of polyaspartic acid derivative and evaluation of its corrosion and scale inhibition performance in seawater utilization. *Desalination* 365, 220–226. doi:10.1016/j.desal.2015.03.006

Gong, S., Li, Y., Li, H., He, L., Yan, Z., Wang, S., et al. (2023). Glutamic acid enhances the corrosion inhibition of polyaspartic acid on q235 carbon steel. *Acs Omega* 8, 39709–39719. doi:10.1021/acsomega.3c05625

Gu, T., Jia, R., Unsal, T., and Xu, D. (2019). Toward a better understanding of microbiologically influenced corrosion caused by sulfate reducing bacteria. *J. Mater Sci. Technol.* 35, 631–636. doi:10.1016/j.jmst.2018.10.026

Hao, X., Dong, J., Etim, I. N., Wei, J., and Ke, W. (2016). Sustained effect of remaining cementite on the corrosion behavior of ferrite-pearlite steel under the simulated bottom plate environment of cargo oil tank. *Corros. Sci.* 110, 296–304. doi:10.1016/j.corsci.2016.04.042

Hasson, D., Shemer, H., and Sher, A. (2011). State of the art of friendly "green" scale control inhibitors: a review article. *Ind. Eng. Chem. Res.* 50, 7601–7607. doi:10.1021/ie200370v

Hegazy, M. A., Abdallah, M., Awad, M. K., and Rezk, M. (2014). Three novel di-quaternary ammonium salts as corrosion inhibitors for api x65 steel pipeline in acidic solution. Part i: experimental results. *Corros. Sci.* 81, 54–64. doi:10.1016/j.corsci.2013.12.010

Jia, R., Tan, J. L., Jin, P., Blackwood, D. J., Xu, D. K., and Gu, T. Y. (2018a). Effects of biogenic h2s on the microbiologically influenced corrosion of c1018 carbon steel by sulfate reducing desulfovibrio vulgaris biofilm. *Corros. Sci.* 130, 1–11. doi:10.1016/j.corsci.2017.10.023

Jia, R., Unsal, T., Xu, D., Lekbach, Y., and Gu, T. (2019). Microbiologically influenced corrosion and current mitigation strategies: a state of the art review. *Int. Biodeterior. Biodegrad.* 137, 42–58. doi:10.1016/j.ibiod.2018.11.007

Jia, R., Yang, D., Xu, D., and Gu, T. (2017). Mitigation of a nitrate reducing pseudomonas aeruginosa biofilm and anaerobic biocorrosion using ciprofloxacin enhanced by d-tyrosine. *Sci. Rep.* 7, 6946. doi:10.1038/s41598-017-07312-7

Jia, R., Yang, D. Q., Bin Abd Rahman, H., and Gu, T. Y. (2018b). An enhanced oil recovery polymer promoted microbial growth and accelerated microbiologically influenced corrosion against carbon steel. *Corros. Sci.* 139, 301–308. doi:10.1016/j.corsci.2018.05.015

Jiang, B., Sun, X., Wang, L., Wang, S., Liu, R., and Wang, S. (2017). Polyethersulfone membranes modified with d-tyrosine for biofouling mitigation: synergistic effect of surface hydrophility and anti-microbial properties. *Chem. Eng. J.* 311, 135–142. doi:10.1016/j.cej.2016.11.088

Kao, W. T. K., Frye, M., Gagnon, P., Vogel, J. P., and Chole, R. (2017). D-amino acids do not inhibit pseudomonas aeruginosa biofilm formation. *Laryngoscope Investig. Otolaryngol.* 2, 4–9. doi:10.1002/lio2.34

Karatan, E., and Watnick, P. (2009). Signals, regulatory networks, and materials that build and break bacterial biofilms. *Microbiol. Mol. Biol. Rev.* 73, 310–347. doi:10.1128/MMBR.00041-08

Knisz, J., Eckert, R., Gieg, L. M., Koerdt, A., Lee, J. S., Silva, E. R., et al. (2023). Microbiologically influenced corrosion-more than just microorganisms. *Fems Microbiol. Rev.* 47, fuad041. doi:10.1093/femsre/fuad041

Kokalj, A. (2023). Considering the concept of synergism in corrosion inhibition. *Corros. Sci.* 212, 110922. doi:10.1016/j.corsci.2022.110922

Kolodkin-Gal, I., Romero, D., Cao, S., Clardy, J., Kolter, R., and Losick, R. (2010). D-amino acids trigger biofilm disassembly. *Science* 328, 627–629. doi:10.1126/science.1188628

Kozlica, D. K., Kokalj, A., and Milošev, I. (2021). Synergistic effect of 2-mercaptobenzimidazole and octylphosphonic acid as corrosion inhibitors for copper and aluminium – an electrochemical, xps, ftir and dft study. *Corros. Sci.* 182, 109082. doi:10.1016/j.corsci.2020.109082

Lam, H., Oh, D., Cava, F., Takacs, C. N., Clardy, J., de Pedro, M. A., et al. (2009). D-amino acids govern stationary phase cell wall remodeling in bacteria. *Science* 325, 1552–1555. doi:10.1126/science.1178123

Li, E., Wu, J., Zhang, D., Sun, Y., and Chen, J. (2018). D-phenylalanine inhibits the corrosion of q235 carbon steel caused by desulfovibrio sp. *Int. Biodeterior. Biodegrad.* 127, 178–184. doi:10.1016/j.ibiod.2017.11.027

Li, E., Wu, J., Zhang, D., Wang, P., Wang, Y., Xu, M., et al. (2021). Electron donor dependent inhibition mechanisms of d-phenylalanine on corrosion of q235 carbon steel caused by desulfovibrio sp. Huiquan2017. *Corros. Sci.* 188, 109493. doi:10.1016/j.corsci.2021.109493

Li, H., Kang, Z., Zhang, K., Gong, S., Zhao, X., Yan, Z., et al. (2023). Enhanced inhibition of hedp on srb-mediated corrosion with d-phenylalanine. *Environ. Res.* 227, 115754. doi:10.1016/j.envres.2023.115754

Liu, H., Wei, J., Dong, J., Chen, Y., Wu, Y., Zhou, Y., et al. (2021). Influence of cementite spheroidization on relieving the micro-galvanic effect of ferrite-pearlite steel in acidic chloride environment. *J. Mater Sci. Technol.* 61, 234–246. doi:10.1016/j.jmst.2020.05.031

Lv, M., Du, M., and Li, Z. (2022). Investigation of mixed species biofilm on corrosion of x65 steel in seawater environment. *Bioelectrochemistry* 143, 107951. doi:10.1016/j.bioelechem.2021.107951

Pu, Y. A., Dou, W. W., Cheng, Y. F., Chen, S. G., Xu, Z. X., and Chen, Z. Y. (2023). Biogenic h2s and extracellular electron transfer resulted in two-coexisting mechanisms in 90/10 cu-ni alloy corrosion by a sulfate-reducing bacteria. *Corros. Sci.* 211, 110911. doi:10.1016/j.corsci.2022.110911

Qian, B., Wang, J., Zheng, M., and Hou, B. (2013). Synergistic effect of polyaspartic acid and iodide ion on corrosion inhibition of mild steel in h2so4. *Corros. Sci.* 75, 184–192. doi:10.1016/j.corsci.2013.06.001

Rott, E., Minke, R., Bali, U., and Steinmetz, H. (2017). Removal of phosphonates from industrial wastewater with uv/feii, fenton and uv/fenton treatment. *Water Res.* 122, 345–354. doi:10.1016/j.watres.2017.06.009

Rott, E., Steinmetz, H., and Metzger, J. W. (2018). Organophosphonates: a review on environmental relevance, biodegradability and removal in wastewater treatment plants. *Sci. Total Environ.* 615, 1176–1191. doi:10.1016/j.scitotenv.2017.09.223

San, N. O., Nazir, H., and Donmez, G. (2014). Microbially influenced corrosion and inhibition of nickel-zinc and nickel-copper coatings by pseudomonas aeruginosa. *Corros. Sci.* 79, 177–183. doi:10.1016/j.corsci.2013.11.004

Saverina, E. A., Frolov, N. A., Kamanina, O. A., Arlyapov, V. A., Vereshchagin, A. N., and Ananikov, V. P. (2023). From antibacterial to antibiofilm targeting: an emerging paradigm shift in the development of quaternary ammonium compounds (qacs). *Acs Infect. Dis.* 9, 394–422. doi:10.1021/acsinfecdis.2c00469

Starosvetsky, D., Khaselev, O., Starosvetsky, J., Armon, R., and Yahalom, J. (2000). Effect of iron exposure in srb media on pitting initiation. *Corros. Sci.* 42, 345–359. doi:10.1016/S0010-938X(99)00088-8

Unsal, T., Ilhan-Sungur, E., Arkan, S., and Cansever, N. (2016). Effects of ag and cu ions on the microbial corrosion of 316l stainless steel in the presence of desulfovibrio sp. *Bioelectrochemistry* 110, 91–99. doi:10.1016/j.bioelechem.2016.03.008

Vahdati, S. N., Behboudi, H., Navasatli, S. A., Tavakoli, S., and Safavi, M. (2022). New insights into the inhibitory roles and mechanisms of d-amino acids in bacterial biofilms in medicine, industry, and agriculture. *Microbiol. Res.* 263, 127107. doi:10.1016/j.micres.2022.127107

Valcarce, M. B., and Vazquez, M. (2010). Phosphate ions used as green inhibitor against copper corrosion in tap water. *Corros. Sci.* 52, 1413–1420. doi:10.1016/j.corsci.2009.12.015

Vasudevan, T., Muralidharan, B., Muralidharan, S., and Iyer, S. V. (1998). Inhibition of corrosion of mild steel in acidic solutions by quaternary salts of pyridinium bases. *Anti-Corros Methods Mater* 45, 120–126. doi:10.1108/00035599810198769

Wang, D., Liu, J., Jia, R., Dou, W., Kumseranee, S., Punpruk, S., et al. (2020). Distinguishing two different microbiologically influenced corrosion (mic) mechanisms using an electron mediator and hydrogen evolution detection. *Corros. Sci.* 177, 108993. doi:10.1016/j.corsci.2020.108993

Wang, D., Wu, H., Li, Z., Wu, Y., Liu, B., Tian, Z., et al. (2024a). Eco-friendly bifunctional antibacterial and anticorrosive broad-spectrum rosin thiourea iminazole quaternary ammonium salt against microbiologically influenced corrosion. *Corros. Sci.* 229, 111847. doi:10.1016/j.corsci.2024.111847

Wang, H., Wang, X., Zhang, Y., Wang, D., Long, X., Chai, G., et al. (2023). Sulfate-reducing bacteria-based bioelectrochemical system for heavy metal wastewater treatment: mechanisms, operating factors, and future challenges. *J. Electroanal. Chem. (Lausanne)* 951, 117945. doi:10.1016/j.jelechem.2023.117945

Wang, Q., Wang, B., Zhou, X., Tan, Z., Zhang, M., Luo, J., et al. (2024b). Effects of carbon source starvation and riboflavin addition on selective corrosion of welded joint by desulfovibrio vulgaris. *Corros. Sci.* 230, 111931. doi:10.1016/j.corsci.2024.111931

Woodard, T. L., Ueki, T., and Lovley, D. R. (2023). H2 is a major intermediate in desulfovibrio vulgaris corrosion of iron. *Mbio* 14, e0007623. doi:10.1128/mbio.00076-23

Xu, D., Gu, T., and Lovley, D. R. (2023). Microbially mediated metal corrosion. *Nat. Rev. Microbiol.* 21, 705–718. doi:10.1038/s41579-023-00920-3

Xu, D., Li, Y., and Gu, T. (2016). Mechanistic modeling of biocorrosion caused by biofilms of sulfate reducing bacteria and acid producing bacteria. *Bioelectrochemistry* 110, 52–58. doi:10.1016/j.bioelechem.2016.03.003

Xu, D., Zhou, E., Zhao, Y., Li, H., Liu, Z., Zhang, D., et al. (2018). Enhanced resistance of 2205 cu-bearing duplex stainless steel towards microbiologically influenced corrosion by marine aerobic pseudomonas aeruginosa biofilms. *J. Mater Sci. Technol.* 34, 1325–1336. doi:10.1016/j.jmst.2017.11.025

Xu, H., and Liu, Y. (2011). D-amino acid mitigated membrane biofouling and promoted biofilm detachment. *J. Membr. Sci.* 376, 266–274. doi:10.1016/j.memsci.2011.04.030

Xu, J., Jia, R., Yang, D., Sun, C., and Gu, T. (2019). Effects of d-phenylalanine as a biocide enhancer of thps against the microbiologically influenced corrosion of c1018 carbon steel. *J. Mater Sci. Technol.* 35, 109–117. doi:10.1016/j.jmst.2018.09.011

Ye, Z., Yang, J., Wang, Z., Zhou, X., Jiang, W., Yi, R., et al. (2023). Mitigating corrosion of deposit-covered carbon steel in solution containing sulfate-reducing bacteria by purging nitrogen. *J. Iron Steel Res. Int.* 30, 1879–1887. doi:10.1007/s42243-022-00853-w

Young, K. D. (2006). The selective value of bacterial shape. *Microbiol. Mol. Biol. Rev.* 70, 660–703. doi:10.1128/MMBR.00001-06

Yu, C., Li, X., Zhang, N., Wen, D., Liu, C., and Li, Q. (2016). Inhibition of biofilm formation by d-tyrosine: effect of bacterial type and d-tyrosine concentration. *Water Res.* 92, 173–179. doi:10.1016/j.watres.2016.01.037

Yu, C., Wu, J., Zin, G., Di Luccio, M., Wen, D., and Li, Q. (2018). D-tyrosine loaded nanocomposite membranes for environmental-friendly, long-term biofouling control. *Water Res.* 130, 105–114. doi:10.1016/j.watres.2017.11.037

Yuan, S., Liang, B., Zhao, Y., and Pehkonen, S. O. (2013). Surface chemistry and corrosion behaviour of 304 stainless steel in simulated seawater containing inorganic sulphide and sulphate-reducing bacteria. *Corros. Sci.* 74, 353–366. doi:10.1016/j.corsci.2013.04.058

Zeino, A., Abdulazeez, I., Khaled, M., Jawich, M. W., and Obot, I. B. (2018). Mechanistic study of polyaspartic acid (pasp) as eco-friendly corrosion inhibitor on mild steel in 3% nacl aerated solution. *J. Mol. Liq.* 250, 50–62. doi:10.1016/j.molliq.2017.11.160

Zhang, B., He, C., Wang, C., Sun, P., Li, F., and Lin, Y. (2015a). Synergistic corrosion inhibition of environment-friendly inhibitors on the corrosion of carbon steel in soft water. *Corros. Sci.* 94, 6–20. doi:10.1016/j.corsci.2014.11.035

Zhang, F., Pan, J., and Claesson, P. M. (2011). Electrochemical and afm studies of mussel adhesive protein (mefp-1) as corrosion inhibitor for carbon steel. *Electrochim Acta* 56, 1636–1645. doi:10.1016/j.electacta.2010.10.033

Zhang, M. Y., He, L., Jin, X., Bai, F., Tong, M. P., and Ni, J. R. (2021). Flagella and their properties affect the transport and deposition behaviors of escherichia coli in quartz sand. *Environ. Sci. Technol.* 55, 4964–4973. doi:10.1021/acs.est.0c08712

Zhang, P., Xu, D., Li, Y., Yang, K., and Gu, T. (2015b). Electron mediators accelerate the microbiologically influenced corrosion of 304 stainless steel by the desulfovibrio vulgaris biofilm. *Bioelectrochemistry* 101, 14–21. doi:10.1016/j.bioelechem.2014.06.010

Zhong, H., Shi, Z., Jiang, G., and Yuan, Z. (2020). Decreasing microbially influenced metal corrosion using free nitrous acid in a simulated water injection system. *Water Res.* 172, 115470. doi:10.1016/j.watres.2020.115470

Zhu, J., Wang, S., Li, H., Qian, J., Lv, L., and Pan, B. (2021). Degradation of phosphonates in co(ii)/peroxymonosulfate process: performance and mechanism. *Water Res.* 202, 117397. doi:10.1016/j.watres.2021.117397